Three-dimensional strain rate in the heart muscle: new insight into cardiac function

Lasse Totland

Supervisor Name

Master's Thesis in Medical Physics
Institue of Experimental Medical Research
Oslo University Hospital
60 ECTS study points

January 22, 2024

Scientific environment

This thesis is carried out at the Institute of Experimental Medical Research, Oslo University Hospital (IEMR, OUS) as part of the study program "Biological and Medical Physics" at the University of Oslo.

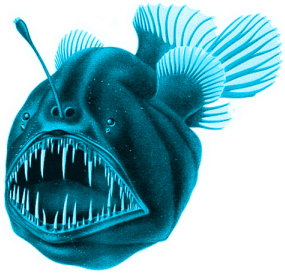

Acknowledgements

Thank someone

Your Name
Place, Date

Abstract

Background: Heart failure (HF) is a crippling and progressive disease, and the main cause of hospitalization among patients over 65 in Europe (1). Left ventricular (LV) strain measurements can be used as an early indicator of myocardial dysfunction after infarct (2). Previous studies have proven the viability of deriving strain rate tensors from motion-encoded MRI (tissue phase mapping, TPM) to describe the direction and magnitude of strain rate on voxel scale (3), though this method has not yet been implemented to investigate heart dysfunction.

Aim: Our aim was to apply this method to gain new insight on regional myocardial function in rat hearts after myocardial infarction using 3D TPM data of the left ventricle with high spatial/temporal resolution.

Materials & Methods: First, to validate the method, a framework developed in Python was used to reproduce global strain and strain rate curves from 2D short-axis cross-sections of the left ventricle that were compared to literature for established methods (4) (5). The framework was then used to assess the 3D direction of strain rate independently from the conventions of radial, circumferential and longitudinal axes as well as the development of these measurements as a function of days after infarction. The measurements were compared to a sham-operated control group.

Results: Global values calculated using our framework agreed well to the literature. Regional analysis revealed that the strain rate magnitude is reduced in the infarcted area and that this area has reduced strain compared to the other wall sections and the sham control curves. Our data also indicate that the strain rate angles, relative to radial direction from heart center, become less homogenous over time after infarct.

Conclusion: We have shown, for the first time, that strain rate tensor analysis of TPM MRI data is a viable tool to assess regional myocardial strain and strain rate in rat hearts. Our framework also allows for measurement of strain rate directions independently of conventional heart geometry, though the implications of our observations here need further investigation.

Contents

Abbreviations

MRI	Magnetic Resonance Imaging
MI	Myocardial Infarction
LV	Left Ventricle
SHAX	Short Axis
PC-MRI	Phase Contrast MRI
TPM	Tissue Phase Mapping
GRS	Global Radial Strain
GCS	Global Circumferential Strain
GLS	Global Longitudinal Strain

Chapter 1

Introduction

1.1 Background

(the effect of HF on society) (what research has been done on HF? methods? (echo, speckle tracking, feature tracking)) (what research lays the foundation of thesis? (Selskog))

1.2 Problem Statement (MI and progression)

(how does regional cardiac function connect to HF progression?) (can strain rate direction tell us something about cardiac function?)

1.3 Aim

(how the thesis plans to answer the questions above) (tensor analysis)

Chapter 2

Theory

This chapter introduces some fundamental MR theory, heart physiology and the mathematics of strain rate tensor calculation.

2.1 MR theory overview

In this section we will establish a basic theoretical foundation of the physics behind MRI. The most prominent atom in the human body is the hydrogen, found in water molecules and many others. The nucleus of a hydrogen atom is a single proton, and for the sake of simplicity we will imagine the human body as a heterogeneous collection of protons where different tissues have different densities.

2.1.1 The spin

In an MRI, a voxel contains signals from the protons within it. To understand how this signal is measured, it is useful to think of the protons as spinning magnetic dipoles. More precisely, we say that these dipoles "precess" around the static B_0-field from the MRI magnet at the Larmor frequency:

$$\omega_0 = \gamma B_0, \tag{2.1}$$

which is proportional to the B_0 field strength, where γ is the gyromagnetic ratio defined by the material. We refer to these dipoles as "spins". Other nuclei with an odd number amount of protons also have a spin property, but hydrogen has a higher γ. This makes it easier to detect, which further supports our simplification that living tissue is a collection of protons.

2.1.2 RF pulse

When an object is placed within the magnet it does not initially produce an interpretable signal. At this point in time, each spin in a voxel precess either parallel or anti-parallel

with the $\vec{B_0}$ field direction. Opposite spins cancel out, and we end up with a vector sum pointing parallel, which represents the Net magnetization vector $\vec{M}$. As long as $\vec{M}$ points parallel to the field, we consider it to be in an equilibrium position. (figure)

Using a orthogonal second field $\vec{B_1}$ to knock $\vec{M}$ out of its equilibrium is what leads us to the signal we need. As $\vec{M}$ is moved down at some angle and its composite spins precess in phase, what separates signal from different tissues is how it recovers back to the rest state via two types of "relaxation". $T1$ relaxation is measured by the time it takes for $\vec{M}$ to become parallel to $\vec{B_0}$ again, and $T2$ relaxation depends on the time it takes for the spins to move out of phase again. Figure () demonstrates how the relaxation of $\vec{M}$ generates a signal that can be measured by a magnetically sensetive reciever coil.

2.1.3 Fourier transform

To interpret the signal ...

2.1.4 K-space

2.1.5 Pulse sequences

2.1.6 Motion encoded MRI / PC-MRI

(venc)

2.2 Heart physiology

2.2.1 Heart anatomy

2.2.2 Cardiac cycle

((Moved from methods, rewrite later) From what we know of LV deformation during the heart cycle, we have some expectations as to how the myocardium should deform. During systole we expect it to compress in the circumferential direction and expand radially during systole as the the heart pumps blood by minimizing the LV cavity. As the heart relaxes and expands again, we expect the opposite. We should be able to observe this from the shapes of the ellipses when plotting over time.)

2.2.3 Myocardial infarction

2.3 Strain and strain rate analysis

This section introduces strain assessment of the heart, some history of the method and different parameters (...)

(strain rate to strain, displacement to strain)

2.4 Strain rate tensor

This section describes how to use velocity gradients to calculate strain rate tensors. Throughout the thesis we will refer to this as the "Selskog method" based on the first author on the article that established the following equations (3).

The n-dimensional velocity gradient tensor ($n \times n$ Jacobian) is calculated like this:

$$L_{ij} = \frac{\partial u_i}{\partial x_j}, \tag{2.2}$$

where u_i, $i = 1, ..., n$ are the velocity components in the x_j direction $j = 1, ..., n$.

The strain rate tensor is then calculated like this:

$$D_{ij} = \frac{1}{2}\left(\frac{\partial u_i}{\partial x_j} + \frac{\partial u_j}{\partial x_i}\right) = \frac{1}{2}\left(L_{ij} + L_{ij}^T\right). \tag{2.3}$$

The eigenvalues λ_i and eigenvectors $\vec{v}_i$ of D_{ij} are the principal values and the principal directions of strain-rate in the myocardium, as shown in Figure 2.1. The sign of the eigenvalue distinguishes between stretching (positive) and compression (negative) in the direction of the corresponding eigenvector.

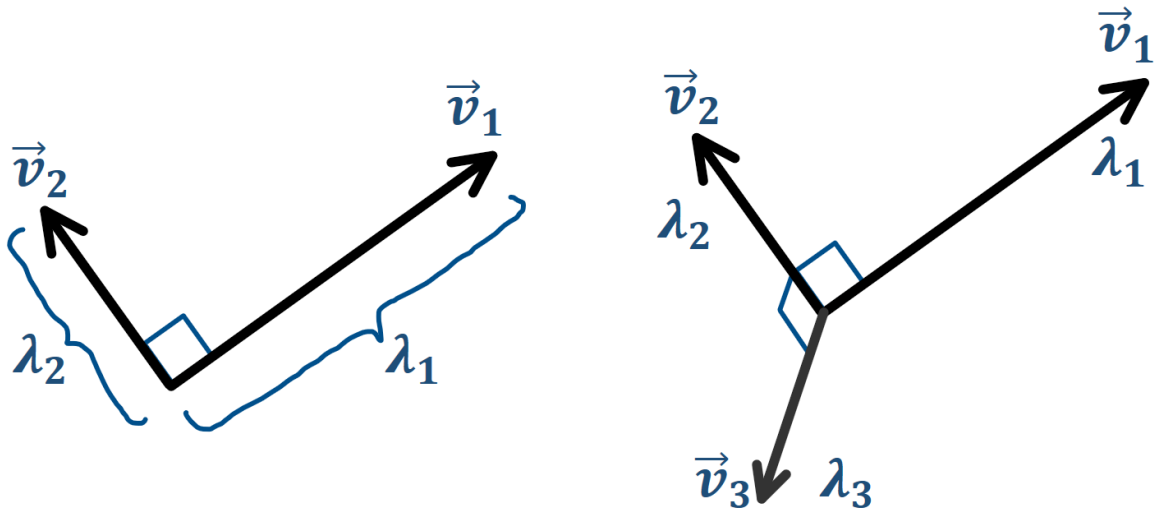

Figure 2.1: Orthogonal eigenvectors $\vec{v}_i$ for a two-dimensional and three-dimensional strain rate tensor D_{ij} (n = 2, n = 3), where the eigenvalues $|\lambda_i|$ represent the vector magnitudes.

The invariant I represents the total amount of strain rate in an n-dimensional strain rate tensor, irrespective of direction:

$$I = \sum_{i=1}^{n} \lambda_i^2. \tag{2.4}$$

Chapter 3

Material & Methods

This chapter will cover the details of the acquisition of our data, preparation for analysis and our methods of analysis including the development of our Python framework.

3.1 Data overview

Here we present a short overview of the data that this thesis is based on. All data used was produced by the Sjaastad group at IEMR in 201x, ...

3.1.1 Rat MI model

Male Wistar-Hannover rats (300 g) were anesthetized (96% O2, and 4% isoflurane) and ventilated by endotracheal intubation using a Zoovent ventilator. In ***N*** of the rats, LV MI was induced by proximal ligation of the left coronary artery during maintained anesthesia (98% O2, and 1.5-2.5% isoflurane). The placement of the ligation was deliberately varied to achieve variable infarct sizes. A Sham-operated control group consisting of ***N*** rats underwent the same procedure with the exception of ligation. All experimental protocols were approved by the Norwegian National Animal Research Authority and performed in accordance with the European Directive 2010/63/EU and institutional guidelines (ID 3284) (14).

3.1.2 MRI Acquisition

In time intervals after operation (1, 3, 10, 21 and 42 days), MRI experiments were performed on a 9.4T magnetic resonance system (Agilent Technologies, Inc) using hardware dedicated to rat cardiac imaging. Anesthesia was induced in a chamber using a mixture of O2 and $\approx 4.0\%$ isoflurane and maintained during acquisition in freely breathing animals using O2 and $\approx 1.5\%$ isoflurane. Throughout the examination, ECG, respiration, and body temperature were monitored, the latter maintained at 37.0°C by heated air. LV short-axis (SHAX) imaging planes were identified from untriggered scout images, and all subsequent acquisitions triggered at the peak of the R wave and

gated for respiratory motion. In all data sets, the temporal resolution was equal to the repetition time.

PC-MRI used an RF-spoiled black blood gradient echo cine sequence using 9-point velocity-encoding (13) and rotating field of view (12). Several SHAX slices were aquired to cover the entire LV. All slices were parallel and shared a common center normal. The PC-MRI time series also covered >100% of the heart cycle. Imaging parameters were echo time TE=2.22 to 2.26 ms, repetition time TR=2.93 to 3.21 ms, field of view FOV=50x50 mm, matrix=128x128, slice thickness Δz=1.5 mm, flip angle=7°, velocity encoding strength=13.9 cm/s, signal averaging=2x using rotating field of view, total acquisition time=45 to 50 minutes.

In each PC-MRI slice, the myocardium was segmented using a semiautomatic method that requires the user to delineate the endo- and epicardium at end systole and end diastole. The masks were then automatically propagated throughout the cardiac cycle based on the underlying velocity fields. Lastly, the myocardial masks were divided into 32 equal sectors defined by the LV center (14).

3.2 TPM data / The velocity field

The TPM data is stored as a large MATLAB structure containing many different fields and parameters.

Relevant to this thesis, we have time dependent velocity fields representing cardiac motion, magnitude fields that represent proton density and relaxation dynamics. The structure also contains a binary mask matrix with the same dimensions as the image with value 0 in voxels determined to be outside the myocardium and value 1 inside, which represents a mask designed during processing.

Relevant static parameters are the time points at end systole T_{es} and end diastole T_{ed} ...

For our analysis, only tissue in the LV is relevant and we have to exclude noisy signal from the movement of blood. This can be achieved by applying the binary mask to reduce all velocities outside the myocardium to zero.

The velocity field in the myocardium is also affected by noise, so we need to smooth the data to compensate for this. For this we can apply the following smoothing function to our velocity field (3):

$$u_{i,smooth} = \frac{(u_i \cdot c) * g}{c * g}, \tag{3.1}$$

where u_i is a velocity field for a spatial component i, and g is a 3D Gaussian function with $\sigma = 2$. Convolution is denoted with a "*". The "c" is defined as a "certainty" matrix, calculated by normalizing the magnitude field to have values in the range $c_k \in [0,\ 1]$ for a voxel k. The intention with the certainty values is to suppress signal from

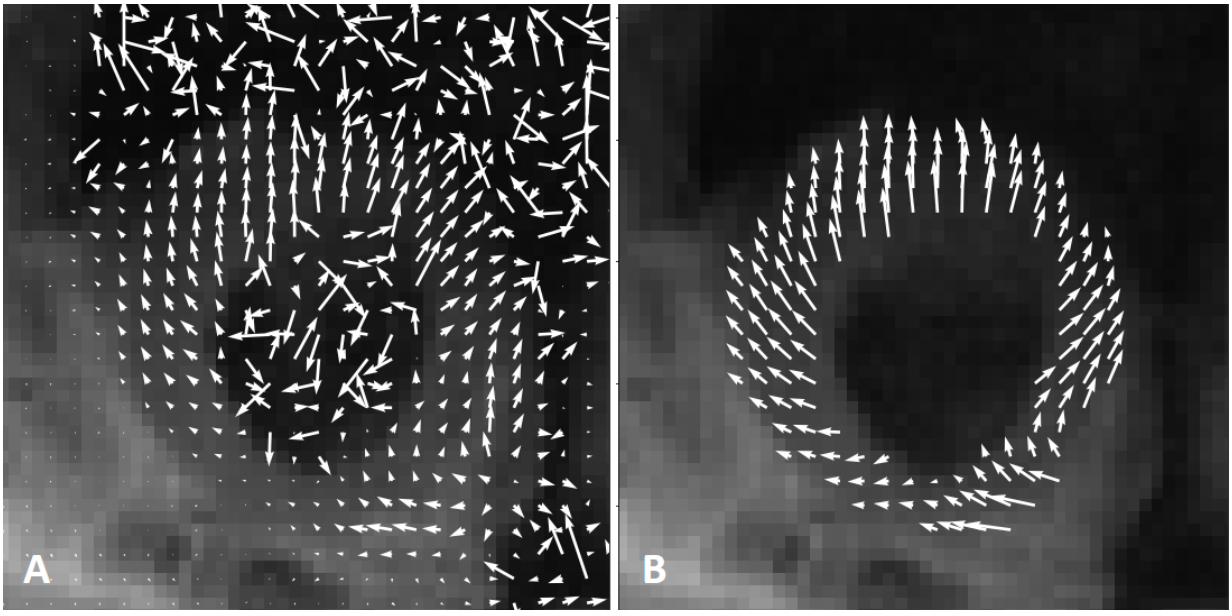

Figure 3.1: A: Velocity field u_i in a 2D SHAX slice in early diastole, including noisy signal in the blood. Magnitude plot in the background. Every other vector is plotted. B: The same field at the same frame but with Equation 3.1 applied ($u_{i,smooth}$) and a binary myocardium mask applied.

the blood, as it produces lower magnitude values than soft tissue, before smoothing with the Gaussian application function.

The effect of smoothing first and *then* applying the mask is demonstrated in Figure 3.1. Seeing the effect of the mask is obvious, but notice how the velocity field within the myocardium becomes more homogenic than in the initial data as well.

3.3 Strain rate tensor analysis framework

This section discusses the process of how our Python framework uses the processed velocity fields to calculate strain rate tensors in the myocardium, visualize them and analyse LV strain rate and strain globally and regionally in the radial, circumferential and longitudinal directions. The framework will also be able to assess the direction of strain rate unrestricted by the conventional axes in heart geometry.

3.3.1 Numeric implementation of Selskog method

With the velocity fields from our TPM data we can calculate strain rate tensors in every voxel at every time point via the Selskog method discussed in Section 2.4. This includes smoothing of the velocity fields prior to any calculations to prevent noise from affecting gradient calculations. A numerical implementation of the velocity gradient, weighted by certainty values, is defined like this (3):

$$\frac{\Delta u_k}{\Delta x} = \frac{c_{k+1}(u_{k+1} - u_k) + c_{k-1}(u_k - u_{k-1})}{\Delta x(c_{k+1} + c_{k-1})}, \tag{3.2}$$

where Δx is the resolution in the direction of the gradient and u_k and c_k are the velocity and certainty in the voxel k. To calculate the strain rate tensor D_{ij} (Equation 2.3) in voxel k in a cartesian 3D velocity field, we need this 3×3 gradient tensor L_{ij} via Equation 2.2:

$$L_{ij} = \begin{bmatrix} \frac{\Delta v_x}{\Delta x} & \frac{\Delta v_x}{\Delta y} & \frac{\Delta v_x}{\Delta z} \\ \frac{\Delta v_y}{\Delta x} & \frac{\Delta v_y}{\Delta y} & \frac{\Delta v_y}{\Delta z} \\ \frac{\Delta v_z}{\Delta x} & \frac{\Delta v_z}{\Delta y} & \frac{\Delta v_z}{\Delta z} \end{bmatrix}, \tag{3.3}$$

where the x- and y-directions are in the SHAX plane and the z-direction is orthogonal and out of plane. For a 2×2 gradient tensor from a 2D field, we simply get:

$$L_{ij} = \begin{bmatrix} \frac{\Delta v_x}{\Delta x} & \frac{\Delta v_x}{\Delta y} \\ \frac{\Delta v_y}{\Delta x} & \frac{\Delta v_y}{\Delta y} \end{bmatrix}. \tag{3.4}$$

To get correct gradient calculations we need to take into account the voxel dimensions in the TPM data, which is especially important in 3D because $\Delta x = \Delta y \neq \Delta z$. From the metadata we find that the slice thickness is $\Delta z = 1.5mm$, while the in-plane voxel resolution is $\Delta x = \Delta y \approx 0.35mm$.

When we apply masks to the velocity fields we exclude voxels that were determined to be outside the myocardium, but the mask borders may still be an issue when calculating gradients. When the strain rate tensor is calculated in a voxel, the gradients require velocity values in adjacent voxels in the gradient direction (as seen in Equation 3.2). If the voxel is positioned right at the edge, one of its neighbors could be outside the mask and exaggerate the gradient value.

The simplest solution to this issue is to exclude the outermost voxels by performing a "binary erosion" of the mask. This shaves off a layer of voxels on the inside and outside edge and ensures that all in-plane gradient calculations are performed completely within the mask. This is demonstrated in Figure 3.2. A solution that would preserve the lost voxels could be to approximate the values just outside of the mask, but erosion still gives us several hundred viable voxels per slice and per frame.

Blood signal is especially an issue when calculating gradients in the z-direction, however. In this case the gradients require velocity values in the slice above and below, and as the radius of the LV masks vary in different positions we get a lot of values outside the masks included in the calculations. The simplest solution to this is to apply Gaussian smoothing to the masked velocity field, letting the signal from the mask borders 'bleed' outside the mask. The values outside now represent to the signal of their nearest neighbours in the mask. (is this a solution to the problem?)

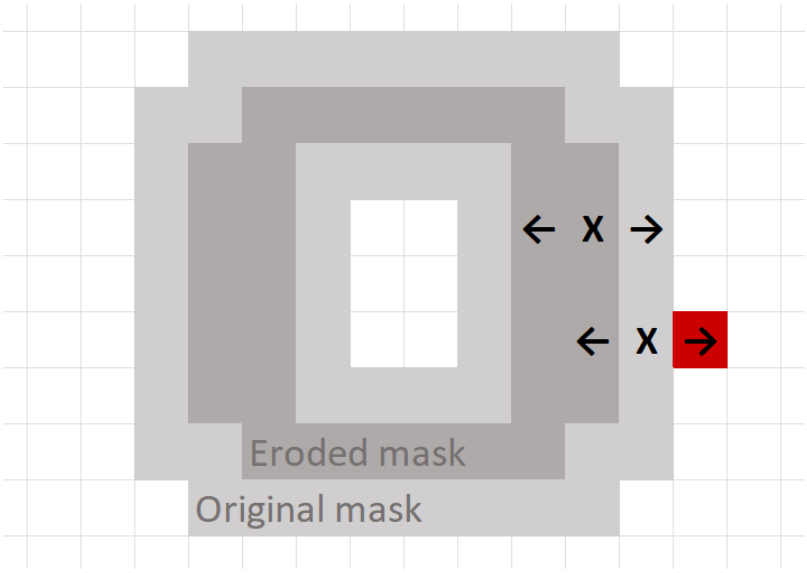

Figure 3.2: A demonstration of binary erosion. For any sampled voxel ("X") in the eroded mask, it will always have neighbors inside the original mask.

3.3.2 Ellipsoid tensor visualization

We now have the tools to calculate strain rate tensors in each voxel of the myocardium for every frame over a full heart cycle. To interpret these tensors, it is useful to visualize them in a way that communicates their direction and magnitude of strain rate.

The eigenvectors of the tensor are orthogonal to each other, and we can use them to span the half-axes of an ellipsoid, or in the two dimensional case: simply an ellipse. The ellipse shape is intended to deform according to the strain rate direction and magnitude that corresponds to its half-axes, meaning that it should expand along the axis where we have stretching (positive values) and contract along the axis with compression (negative) or have a roughly spherical shape when the magnitude is around zero. Figure 3.3 illustrates this.

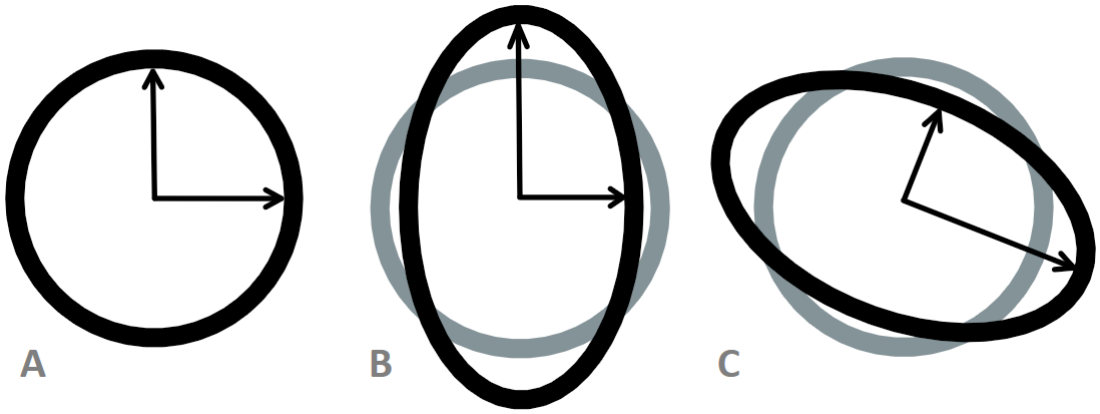

Figure 3.3: Ellipses spanned by eigenvectors of various magnitudes and directions. A: magnitudes around zero; no deformation gives a circular shape. B, C: Stretch and compression give elliptic shapes.

We expect to see compression along one eigenvector and expansion along the other for

the majority of 2D strain rate tensors due to the assumption of the heart tissue being incompressible and assuming conservation of mass.

To create this visual, we can transform the magnitudes to force the tensors to be positive definite (15). We have chosen to use the function $w(\lambda_i) = tanh(\lambda_i) + 1$ where λ_i is some eigenvalue. This transforms the half-axes with positive eigenvalues to have lengths in the range $w \in (1.0,\ 2.0)$, the negative values to have values in the range $w \in (0.0,\ 1.0)$ and ensures that $w(0) = 1$.

Keep in mind that this function is only applied as a *visual* tool for the ellipse plotting, and not in the quantitative analysis. This means that the constants above are somewhat arbitrary and could be scaled for visibility, but the point is that it produces the correct ellipse proportions and normalizes the scale to make the low magnitude tensors clearly visible. The same principle goes for 3D strain rate tensors too, but with an ellipsoid spanned by three orthogonal eigenvectors.

To more effectively communicate the regional variation in strain rate direction and magnitude visually, we can assign these parameters to a color range and opacity of the ellipses. When discussion the direction of some tensor in the myocardium, we are interested in angles θ_i of the eigenvectors relative to radial direction as demonstrated in Figure 3.4. Here we also demonstrate that it is the alignment of the ellipse relative to the radial and tangential axes that tells us about the strain rate. In other words, if you flip any of the eigenvectors 180° the direction still correctly describes the direction of strain rate.

This means that all possible ellipse alignments can be described by the range $\theta_i \in [0,\ 90]°$, where 0° represents radial alignment and 90° tangential alignment, and we will use this to scale the ellipses to a color gradient. The opacity will be assigned to the total amount of strain rate I via Equation 2.4.

3.3.3 Eigenvector decomposition

The angles θ_i will not only be used for visual analysis, but will also be used to gather quantitative information. Vector decomposition, using the eigenvector angles θ_i and eigenvalues λ_i as vector length, can be used to find the radial and tangential components of the strain rate of a tensor r_i and c_i. We interpret the tangential component as the circumferential strain rate. These components are simple to find using the trigonometric formulas for right triangles, which we can construct with the eigenvalue λ_i as the hypotenuse and r_i and c_i as the catheti. This is shown in Figure 3.5.

For a slice at some time-point in our MR recording we generally have hundreds of valid voxels to sample, so we need some way of organizing the data we collect from the tensors. When using 2D strain rate tensors to analyze a group of voxels, the whole LV or a smaller sector, we are interested in their sum total contribution to radial and circumferential strain rate where the contribution from one tensor is as demonstrated in Figure 3.5.

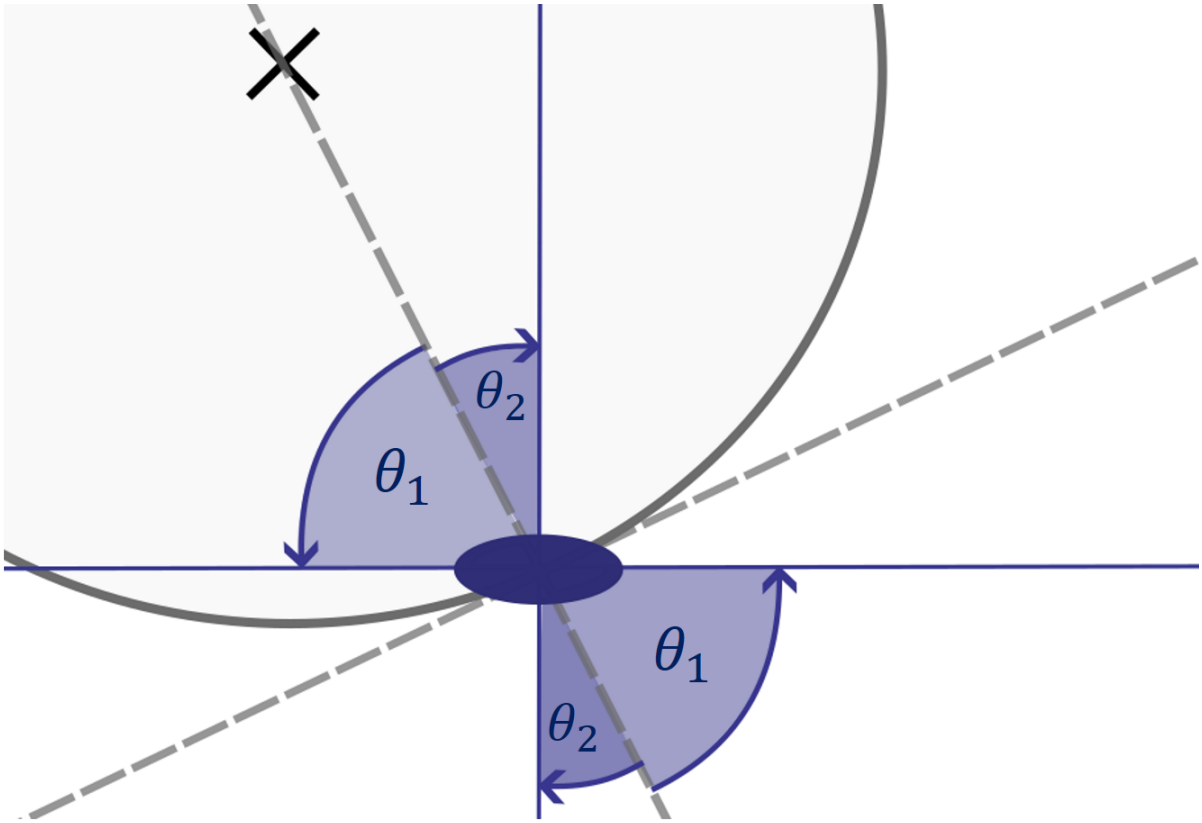

Figure 3.4: Diagram of an ellipse positioned in a coordinate system defined by radial and tangential axes (dashed lines) defined by a model of LV circumference and center ("X"). The ellipse half-axes, representing the tensor eigenvectors $\vec{v}_1$ and $\vec{v}_2$, are oriented with angles θ_1 and θ_2 with respect to the radial axis.

3.3.4 Global LV strain rate

When plotting the net total radial and circumferential strain rate for all of the time-points of velocity data in the whole LV, we expect to see curves resembling the global strain rate curves as seen in (**theory section**). Whether we get a positive or negative peak depends on the sums of positive and negative eigenvalues that contribute in the radial and circumferential directions.

To get correct peak values, we need to make sure that the units are scaled correctly throughout the calculation process. Firstly, we need to keep count of the amount of tensors generated in the LV at any frame as the myocardium mask changes shape throughout the cardiac cycle. Dividing the total strain rate for this frame by this amount means we get an average measurement and prevent larger LV cross-sections from giving 'more' signal because it has more voxels. Secondly, the units of the velocity components are cm/s, and we want strain rate measured in the unit s^{-1} which means all spatial and temporal variables should be converted to cm and s.

Previously, we have smoothed the velocity field in the SHAX xy-plane, but we have not yet smoothed our data in the time dimension. We expect the curves to be noisy because of this. To solve this we simply apply a running average smoothing function on the strain rate curves. The running average function convolves the curve with a kernel of

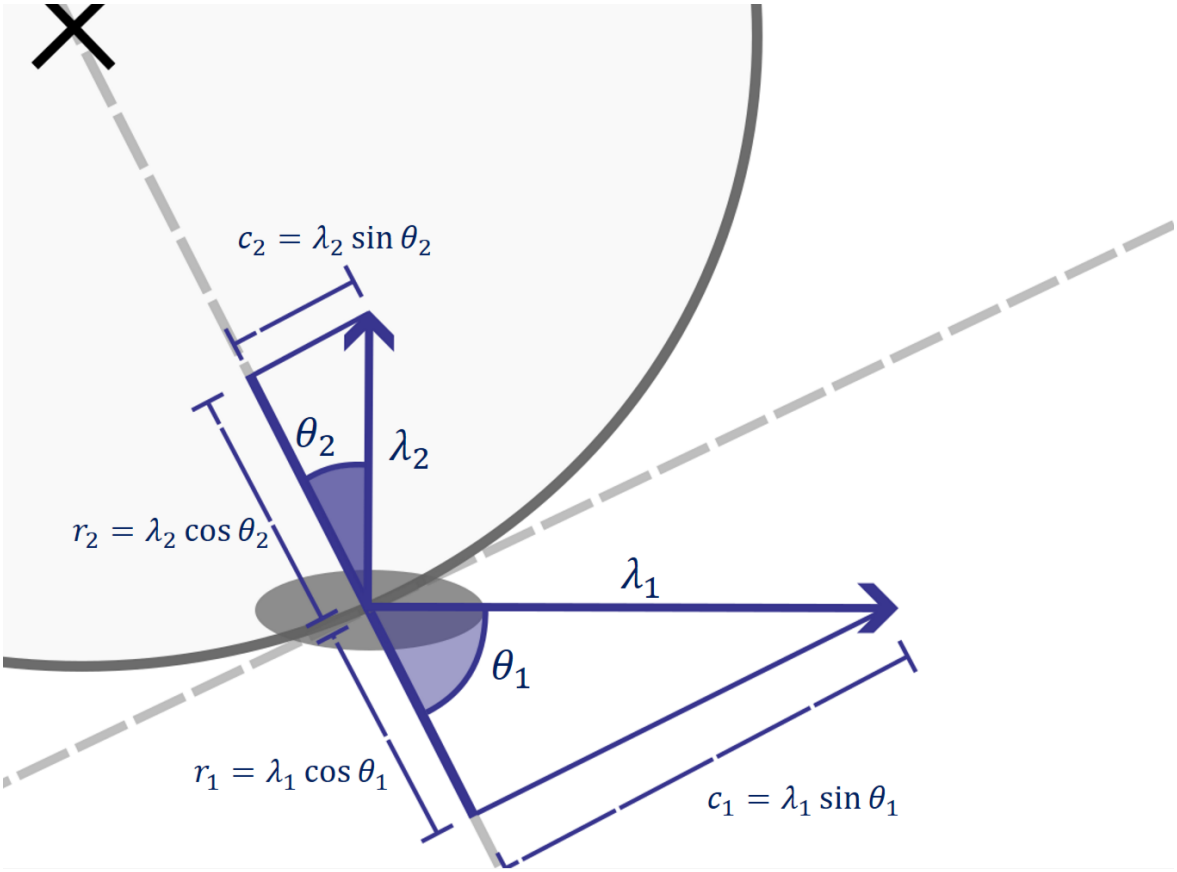

Figure 3.5: The eigenvectors represented by the ellipse in Figure 3.4 in the same system. Radial and circumferential components r_i and c_i are defined by corresponding θ_i and λ_i.

length $N = 2,4,6...$ with elements $1/N$. For $N = 4$ a datapoint is transformed to the average of itself and its 4 surrounding points within the kernel. (... elaborate? figure?)

(notes to self:) (running average N = 4, experiment with lower values? does higher N suppress peaks more strongly? how does mode=valid affect analysis? does the order of V smoothing (mask before or after) affect peak values?)

3.3.5 Global LV strain

From theory section (...) we know that we can find strain from time-integrating strain rate. In our framework we use cumulative trapezoidal numerical integration to produce strain curves from our strain rate curves. Specifically, we use the "cumtrapz" function from the SciPy module. The unit will be %, representing relative deformation from the initial time-point.

There are more things to consider than just integrating, however. Despite smoothing the data, it will still be affected by background noise which accumulates during integration. The effect of this is that the strain curve values become increasingly distorted by the accumulating noise. We can work around this based on assuming that the strain curves are cyclic from the initial time-point to end-diastole.

When integrating, we set the initial value to 0. The strain value we find at end diastole

will likely not have returned to zero due to the noise, but we do some subtle changes to force this boundary condition. Firstly, we produce two strain curves; one that is integrated forward in time and one the other way. The weighted average sum of these two functions should now be affected by noise equally at the beginning and end of the cardiac cycle.

Secondly, we apply a weighting function that equals to 1 for the majority of the duration, but cuts off to 0 toward the beginning and end of the cardiac cycle. This step is mostly for the visuals, and gives us strain curves that look cyclic by starting and stopping at 0 without affecting the peak values.

3.3.6 Regional strain and strain rate

To perform regional strain and strain rate analysis, we want to divide the LV into sections that can be analyzed separately. From the TPM data structure we can find time-dependent sector maps with the same dimensions as the image and velocity matrices that assign every voxel to one of 36 sectors as shown in Figure 3.6A. Hearts with visible infarction will also include infarct sectors in the metadata designed during processing. In the case of the figure, the metadata would contain a tuple "$(1, 10)$" representing an infarct sector range from 1 to 10.

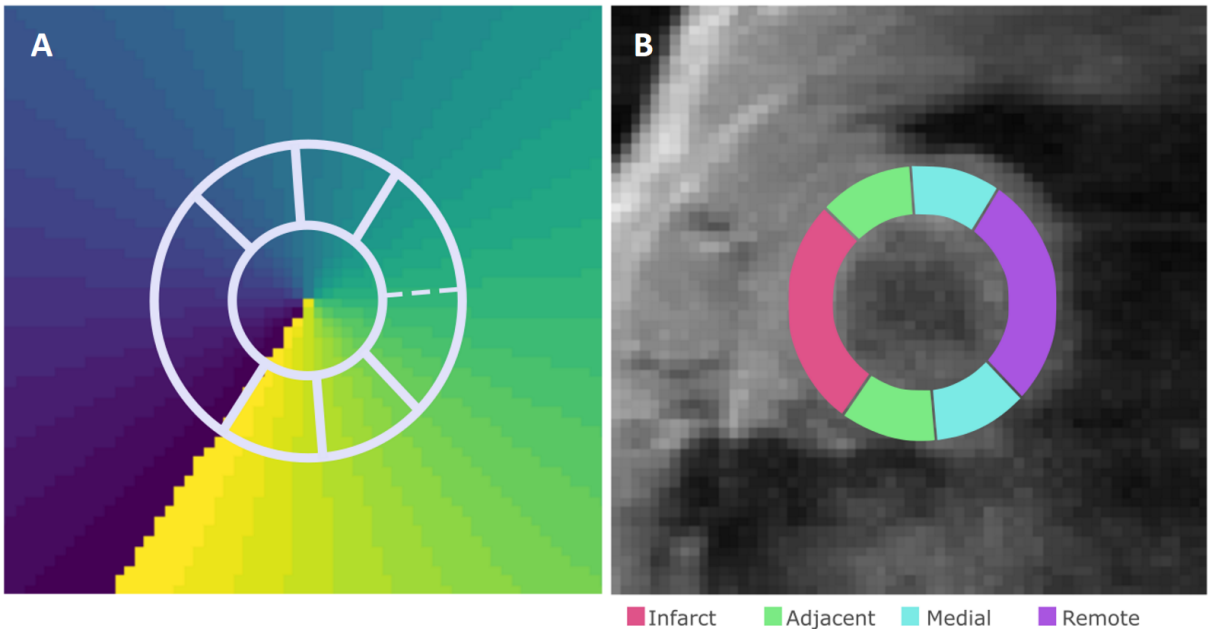

Figure 3.6: A: Sector map plotted as a clockwise color scale from sector 1 to 36, divided by isotropic lines from the LV center. Different LV sections are outlined where the largest (from sector 1 to 10) represents the infarct sectors of this heart. The rest is divided into 6 equal parts. B: Sector groups color coded based on infarct proximity.

For the infarcted hearts, we want the infarct sectors to be part of one group. The remaining LV will be split into six and distributed to three groups based on proximity to the infarct sectors: adjacent, medial, remote (5). This is shown in Figure 3.6B. If the remaining sector amount is not divisible by 6 we round down to the closest number that is and give remaining sectors to the remote group.

A unique issue happens when both sector 1 and 36 is in a group we are checking for viable voxels, which is very likely. This means that this sequence will have a reverse range like for example $[32, 6]$, which Python struggles to interpret. A simple trick to solve this is to also check if the voxel is *not* in the range $[6, 32]$.

The Sham control group will of course not have infarct sectors, and some in the MI group as well if there was no visible infarct in the MRI. In these cases, we choose an arbitrary infarct sector range and rename the groups to "Group 1" and so on. We have chosen to define Group 1 by the range $[4, 13]$ which ensures that the four groups have approximately covers the same amount of sectors.

We can now perform strain and strain rate analyses like we did for the whole LV with each of these groups, which lets us observe regional variation quantitatively between the groups by measuring standard deviation between peak values. We can also assess dyssynchrony between the groups by measuring the standard deviation of the peak time-points in the strain curves.

3.3.7 Eigenvector angle distributions

The analysis described thus far relies on the vector decomposition in the radial and circumferential direction in our LV model.

3.3.8 Framework adjustments for 3D analysis

(establish how I define phi etc)

(move all mentions of 3d sr tensors here?)

3.4 3D strain rate tensor analysis

3.4.1 (phi)

3.4.2 Longitudinal strain rate

3.5 Correlation analysis

Chapter 4

Results

This chapter presents the results produced by our Python framework. We have produced strain rate, strain, and eigenvector angle data for Sham and MI rat hearts and collected curve parameters that were used in statistical analysis to look for correlations with MI progression and heart function. We separate the analyses using 2D and 3D strain rate tensors in respective sections due to...

4.1 2D strain rate tensor analysis

4.1.1 Visualization

Figure 4.1 demonstrates the ellipse plot framework in action in two different time points, showing 2D strain rate tensors represented within the mask. Every other voxel is sampled in this case, or in other words: they are sampled in a grid with spacing of one voxel for the sake of visibility. For quantitative results, however, we always utilize all viable voxels within the myocardium.

We see that ... (discussion?)

4.1.2 Global strain rate

4.1.3 Global strain

4.1.4 Regional strain

Figure 4.2 ...

4.1.5 Eigenvector angle distribution

4.1.6 Progression / statistical analysis

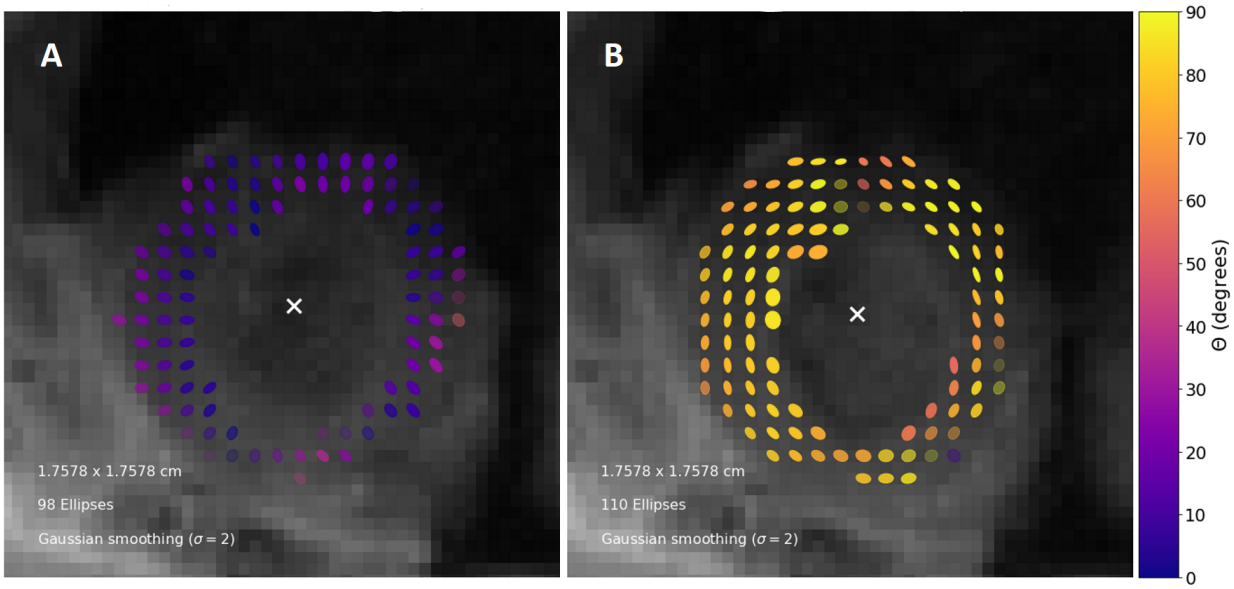

Figure 4.1: Ellipse plots with color scale defined by direction of stretch relative to the radial direction from the heart center (marked 'X')). The ellipse opacity corresponds to the invariant $I = \lambda_1^2 + \lambda_2^2$ from Equation 2.4. A: Mid systole, with the myocardium experiencing stretching in the radial direction and compression in the circumferential direction. B: Early diastole, stretch along the circumferential direction and compression in the radial.

4.2 3D strain rate tensor analysis

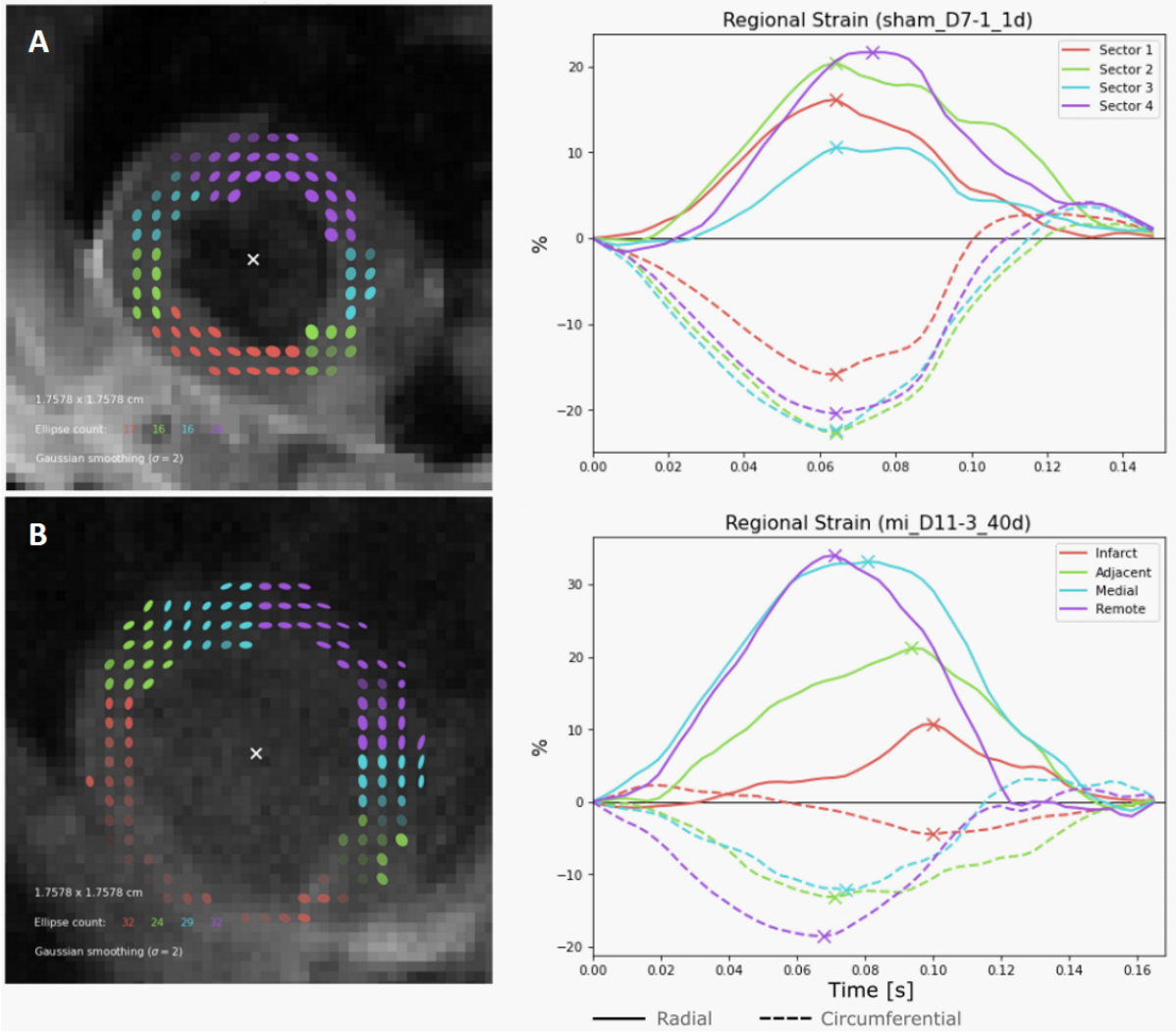

Figure 4.2: Regional strain analysis of a Sham and MI heart, featuring strain rate tensor ellipse plots at early diastole and strain plots with color coding based on group. A: Sham heart with arbitrary, numerated sectors. B: MI heart 40 days after infarction, sectors based on infarct sector and proximity.

Chapter 5

Discussion

Chapter 6

Conclusion

Bibliography

[1] J. G. Cleland, K. Swedberg, F. Follath, M. Komajda, A. Cohen-Solal, J. C. Aguilar, R. Dietz, A. Gavazzi, R. Hobbs, J. Korewicki, H. C. Madeira, V. S. Moiseyev, I. Preda, W. H. van Gilst, J. Widimsky, N. Freemantle, J. Eastaugh, and J. Mason. The euroheart failure survey programme– a survey on the quality of care among patients with heart failure in europe. part 1: patient characteristics and diagnosis. *Eur Heart J*, 24(5):442–63, 2003. (document)

[2] F. Valente, L. Gutierrez, L. Rodriguez-Eyras, R. Fernandez, M. Montano, A. Sao-Aviles, V. Pineda, A. Guala, H. Cuellar, A. Evangelista, and J. Rodriguez-Palomares. Cardiac magnetic resonance longitudinal strain analysis in acute st-segment elevation myocardial infarction: A comparison with speckle-tracking echocardiography. *Int J Cardiol Heart Vasc*, 29:100560, 2020. (document)

[3] P. Selskog, E. Heiberg, T. Ebbers, L. Wigström, and M. Karlsson. Kinematics of the heart: strain-rate imaging from time-resolved three-dimensional phase contrast mri. *IEEE Trans Med Imaging*, 21(9):1105–9, 2002. (document), 2.4, 3.2, 3.3.1

[4] C. Mátyás, A. Kovács, B. T. Németh, A. Oláh, S. Braun, M. Tokodi, B. A. Barta, K. Benke, M. Ruppert, B. K. Lakatos, B. Merkely, and T. Radovits. Comparison of speckle-tracking echocardiography with invasive hemodynamics for the detection of characteristic cardiac dysfunction in type-1 and type-2 diabetic rat models. *Cardiovasc Diabetol*, 17(1):13, 2018. (document)

[5] T. Røe Å, M. Ruud, E. K. Espe, O. Manfra, S. Longobardi, J. M. Aronsen, E. S. Nordén, T. Husebye, T. R. S. Kolstad, A. Cataliotti, G. Christensen, O. M. Sejersted, S. A. Niederer, GØ Andersen, I. Sjaastad, and W. E. Louch. Regional diastolic dysfunction in post-infarction heart failure: role of local mechanical load and serca expression. *Cardiovasc Res*, 115(4):752–764, 2019. (document), 3.3.6

[6] V. M. Almaas, K. H. Haugaa, E. H. Strom, H. Scott, H. J. Smith, C. P. Dahl, O. R. Geiran, K. Endresen, S. Aakhus, J. P. Amlie, and T. Edvardsen. Noninvasive assessment of myocardial fibrosis in patients with obstructive hypertrophic cardiomyopathy. *Heart*, 100(8):631–8, 2014.

[7] M. S. Amzulescu, M. De Craene, H. Langet, A. Pasquet, D. Vancraeynest, A. C. Pouleur, J. L. Vanoverschelde, and B. L. Gerber. Myocardial strain imaging:

review of general principles, validation, and sources of discrepancies. *Eur Heart J Cardiovasc Imaging*, 20(6):605–619, 2019.

[8] B. A. Bendiksen, G. McGinley, I. Sjaastad, L. Zhang, and E. K. S. Espe. A 4d continuous representation of myocardial velocity fields from tissue phase mapping magnetic resonance imaging. *PLoS One*, 16(3):e0247826, 2021.

[9] X. Chen, J. Pan, J. Shu, X. Zhang, L. Ye, L. Chen, Y. Hu, and R. Yu. Prognostic value of regional strain by cardiovascular magnetic resonance feature tracking in hypertrophic cardiomyopathy. *Quant Imaging Med Surg*, 12(1):627–641, 2022.

[10] X. Chen, J. Pan, J. Shu, X. Zhang, L. Ye, L. Chen, Y. Hu, and R. Yu. Prognostic value of regional strain by cardiovascular magnetic resonance feature tracking in hypertrophic cardiomyopathy. *Quant Imaging Med Surg*, 12(1):627–641, 2022.

[11] N. D'Elia, J. D'Hooge, and T. H. Marwick. Association between myocardial mechanics and ischemic lv remodeling. *JACC Cardiovasc Imaging*, 8(12):1430–1443, 2015.

[12] E. K. Espe, J. M. Aronsen, K. Skardal, J. E. Schneider, L. Zhang, and I. Sjaastad. Novel insight into the detailed myocardial motion and deformation of the rodent heart using high-resolution phase contrast cardiovascular magnetic resonance. *J Cardiovasc Magn Reson*, 15(1):82, 2013. 3.1.2

[13] E. K. Espe, J. M. Aronsen, B. Skrbic, V. M. Skulberg, J. E. Schneider, O. M. Sejersted, L. Zhang, and I. Sjaastad. Improved mr phase-contrast velocimetry using a novel nine-point balanced motion-encoding scheme with increased robustness to eddy current effects. *Magn Reson Med*, 69(1):48–61, 2013. 3.1.2

[14] E. K. S. Espe, J. M. Aronsen, M. Eriksen, O. M. Sejersted, L. Zhang, and I. Sjaastad. Regional dysfunction after myocardial infarction in rats. *Circ Cardiovasc Imaging*, 10(9), 2017. 3.1.1, 3.1.2

[15] H. Haraldsson, L. Wigstrom, M. Lundberg, A. F. Bolger, J. Engvall, T. Ebbers, and J. P. Kvitting. Improved estimation and visualization of two-dimensional myocardial strain rate using mr velocity mapping. *J Magn Reson Imaging*, 28(3):604–11, 2008. 3.3.2

[16] M. Ruppert, B. K. Lakatos, S. Braun, M. Tokodi, C. Karime, A. Olah, A. A. Sayour, I. Hizoh, B. A. Barta, B. Merkely, A. Kovacs, and T. Radovits. Longitudinal strain reflects ventriculoarterial coupling rather than mere contractility in rat models of hemodynamic overload-induced heart failure. *J Am Soc Echocardiogr*, 33(10):1264–1275 e4, 2020.

[17] T. J. Samuel, A. P. Oneglia, D. J. Cipher, J. A. Ezekowitz, J. R. B. Dyck, T. Anderson, J. G. Howlett, D. I. Paterson, R. B. Thompson, and M. D. Nelson. Integration of longitudinal and circumferential strain predicts volumetric change across the cardiac cycle and differentiates patients along the heart failure continuum. *J Cardiovasc Magn Reson*, 25(1):55, 2023.

[18] R. Tanacli, D. Hashemi, T. Lapinskas, F. Edelmann, R. Gebker, G. Pedrizzetti, A. Schuster, E. Nagel, B. Pieske, H. D. Düngen, and S. Kelle. Range variability in cmr feature tracking multilayer strain across different stages of heart failure. *Sci Rep*, 9(1):16478, 2019.

Appendix A